Stereo-Active Lone-Pair Control on the Ferromagnetic Behavior in VO(SeO$_2$OH)$_2$: A New Acentric Ferromagnetic Material

Sang-Hwan Kim,[†] Jeongho Yeon,[†] Athena S. Sefat,[‡] David G. Mandrus,[§] and
P. Shiv Halasyamani*,[†]

[†]*Department of Chemistry, University of Houston, 136 Fleming Building, Houston, Texas 77204-5003,
United States,* [‡]*Materials Science and Technology Division, Oak Ridge National Laboratory,
Oak Ridge, Tennessee 37831, United States, and* [§]*Department of Materials Science and Engineering,
The University of Tennessee, Knoxville, Tennessee 37996, United States*

A new acentric ferromagnetic material, VO(SeO$_2$OH)$_2$, has been synthesized and characterized by single crystal X-ray diffraction, second harmonic generation (SHG), and magnetization measurements. The crystal structure of VO(SeO$_2$OH)$_2$ consists of linear chains of corner-shared V^{4+}O$_6$ octahedra that are connected by SeO$_2$OH groups. The material exhibits a weak SHG efficiency, comparable to α-SiO$_2$, and a ferromagnetic transition (T_C) at ∼2.5 K with a saturated magnetic moment of 1.09 μ_B per formula unit (μ_B/FU). The origin of the ferromagnetism is explained by the suppression of the antiferromagnetic superexchange (SE) and supersuper-exchange (SSE) interactions in the *intra*-chain and *inter*-chain magnetic interactions, respectively. In addition, using first principles density functional theory (DFT) calculations, we show that the SSE interactions depend on the O(2)−Se^{4+}−O(3) angle. As we demonstrate, the stereoactive lone-pair on Se^{4+} is the driving force for the *inter*-chain ferromagnetic interactions.

Introduction

In oxides, the lone-pair associated with main group metals, for example, Se^{4+}, Te^{4+}, I^{5+}, and so forth, is of topical interest attributable to their inclusion in materials that exhibit functional properties such as multiferroic behavior, ferroelectricity, and second-order nonlinear optical behavior.[1−6] With these cations, the stereoactive lone-pair creates a highly asymmetric and locally polar coordination environment.[7−9] This coordination environment may be exploited with respect to magnetoelectric behavior, where magnetic ordering is observed in conjunction with macroscopic and reversible polarization

(ferroelectric behavior), for example, BiFeO$_3$ and PbVO$_3$.[10−15] The magnetic ordering is attributable to the indirect interactions between the transition metal cations, Fe^{3+} and V^{4+} through O$^{2−}$, respectively. The magnetic interactions are well understood through the Goodenough−Kanamori (GK) rules[16,17] where the symmetry and the electron occupancy of the interacting orbitals on pairwise neighboring magnetic centers are considered to understand the magnetic ground state. The great success of the GK rules was recognized as superexchange (SE) interactions are critically dependent on structural variations. For example, ferromagnetic interactions in edge-shared magnetic octahedra, M$_2$O$_{10}$, are favored when superexchange (SE) interactions between the "magnetic" cations are reduced, that is, when the M−O−M angle is close to 90°.[16−18] Despite the remarkable success of the GK rules, what is not well understood is magnetic behavior led by supersuper-exchange (SSE) interactions that are mediated through complex nonmagnetic groups such as lone-pair polyhedra (SeO$_3$, TeO$_3$, etc).[19,20] In addition, it is worth investigating any

---

*To whom correspondence should be addressed. E-mail: psh@uh.edu.

(1) Lines, M. E.; Glass, A. M. *Principles and Applications of Ferroelectrics and Related Materials*; Oxford University Press: Oxford, 1991.
(2) Halasyamani, P. S.; Poeppelmeier, K. R. *Chem. Mater.* **1998,** *10,* 2753.
(3) Halasyamani, P. S. *Chem. Mater.* **2004,** *16,* 3586.
(4) Stoltzfus, M. W.; Woodward, P. M.; Seshadri, R.; Klepeis, J.-H.; Bursten, B. *Inorg. Chem.* **2007,** *46,* 3839.
(5) Khomskii, D. *Physics* **2009,** *2,* 20.
(6) Seshadri, R.; Hill, N. A. *Chem. Mater.* **2001,** *13,* 2892.
(7) Sidgwick, N. V.; Powell, H. M. *Proc. R. Soc. London, Ser. A* **1940,** *176,* 153.
(8) Gillespie, R. J.; Nyholm, R. S. *Q. Rev., Chem. Soc* **1957,** *11,* 339.
(9) Galy, J.; Meunier, G.; Andersson, S.; Astrom, A. *J. Solid State Chem.* **1975,** *13,* 142.
(10) Kiselev, S. V.; Ozerov, R. P.; Zhdanov, G. S. *Doklady Akademii Nauk SSSR* **1962,** *145,* 1255.
(11) Kubel, F.; Schmid, H. *Acta Crystallogr.* **1990,** *B46,* 698.
(12) Shpanchenko, R. V.; Chernaya, V. V.; Tsirlin, A. A.; Chizhov, P. S.; Sklovsky, D. E.; Antipov, E. V.; Khlybov, E. P.; Pomjakushin, V.; Balagurov, A. M.; Medvedeva, J. E.; Kaul, E. E.; Geibel, C. *Chem. Mater.* **2004,** *16,* 3267.
(13) Singh, D. J. *Phys. Rev. B: Condens. Matter* **2006,** *73,* 094102/1.

(14) Kumar, A.; Martin, L. W.; Denev, S.; Kortright, J. B.; Suzuki, Y.; Ramesh, R.; Gopalan, V. *Phys. Rev. B: Condens. Matter* **2007,** *75,* 060101/1.
(15) Martin, L. W.; Zhan, Q.; Suzuki, Y.; Ramesh, R.; Chi, M.; Browning, N.; Mizoguchi, T.; Kreisel, J. *Appl. Phys. Lett.* **2007,** *90,* 062903/1.
(16) Kanamori, J. *Phys. Chem. Solids* **1959,** *10,* 87.
(17) Goodenough, J. B. *Magnetism and the Chemical Bond*; Interscience: New York, 1963.
(18) Anderson, P. W. *Solid State Phys.* **1963,** *14,* 99.
(19) Trombe, J. C.; Gleizes, A.; Galy, J.; Renard, J. P.; Journaux, Y.; Verdaguer, M. *New J. Chem.* **1987,** *11,* 321.

analogies between SE and SSE interactions associated with the GK rules.

Recently, Kim et al.[20] have reported the reinvestigation of the magnetic properties of $VOSe_2O_5$ (tetragonal, space group $P4cc$, $Z = 8$) where the linear chains of corner-shared VO_6 octahedra are aligned in a square lattice. The chains are *all* connected to each other along the sides and the diagonals of the square by one lone-pair Se_2O_5 group. $VOSe_2O_5$ exhibits a ferrimagnetic ground state through three magnetic transitions, and shows frequency dependent magnetic behavior at lower temperatures. These complicated magnetic properties were explained through the lone-pair Se_2O_5 group that provides *inter*-chain magnetic interaction paths, for example, SSE interactions. The explanation described how critically the lone-pair Se_2O_5 groups contribute to the SSE interactions. For deeper insight, our aim was to discover a somewhat simpler material whose magnetic interactions are mediated through lone-pair groups.

In our effort to find new V^{4+} magnetic materials, $VO(SeO_2OH)_2$ (tetragonal, space group $P\overline{4}2_1c$, $Z = 4$) was discovered through the use of oxalic acid dihydrate ($C_2H_2O_4 \cdot 2H_2O$) as a mild reducing reagent. $VO(SeO_2OH)_2$ exhibits a somewhat simpler structure compared to $VOSe_2O_5$ (see Figure 1). In $VO(SeO_2OH)_2$, linear chains of corner-shared VO_6 octahedra are aligned in a square lattice, that are *only* connected along the sides by one lone-pair SeO_2OH group. Interestingly, ferromagnetic transition ($T_C = \sim 2.5$ K) is observed with a saturated magnetic moment of 1.09 μ_B/FU. The magnetic coupling constants for *intra*-chain and *inter*-chain interactions were evaluated through first-principles density functional theory (DFT) calculations. Subsequently, we demonstrate for the first time that the *inter*-chain interactions, for example, the SSE interactions, are dependent on the $O–Se^{4+}–O$ angle in the lone-pair SeO_2OH group. The critical role of the stereoactive lone-pair on Se^{4+} is described analogous to the GK rules.[18,21,22] In this paper, we report on the synthesis, crystal structure, second harmonic generation (SHG), magnetic properties, electronic structure calculations, and structure–property relationships of a new *acentric ferromagnetic* material, $VO(SeO_2OH)_2$.

Experimental Details

Reagents. V_2O_5 (Alfa Aesar, 99.6%), SeO_2 (Alfa Aesar, 99.4%), and $C_2H_2O_4 \cdot 2H_2O$ (Alfa Aesar, 98%) were used as received.

Synthesis. $VO(SeO_2OH)_2$ was discovered utilizing oxalic acid dihydrate ($C_2H_2O_4 \cdot 2H_2O$) as low melting flux (melting point $T_m = 101–102$ °C) as well as a mild reducing reagent.[23] $VO(SeO_2OH)_2$ was prepared by combining V_2O_5 (0.181 g, 1.00 mmol), SeO_2 (0.221 g, 4.00 mmol), and $C_2H_2O_4 \cdot 2H_2O$ (0.127 g,
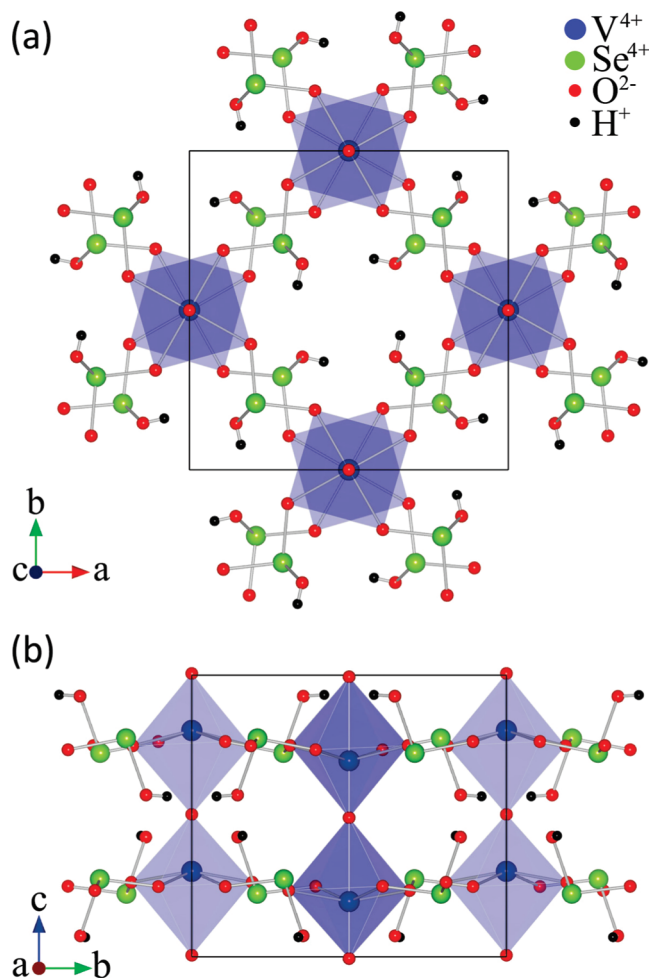

Figure 1. Ball-and-stick representation of $VO(SeO_2OH)_2$ in the (a) *ab*-plane and (b) *bc*-plane. For clarity, the full occupation of V(1) is assumed.

1.00 mmol). The mixture was thoroughly ground, pressed into a pellet, and placed in a 23 mL Teflon-lined autoclave. Mixing the reagents thoroughly was determined to be important in obtaining the highest possible yield of $VO(SeO_2OH)_2$. No additional liquid, water, acid, or base, was added to the autoclave. The autoclave was closed, heated to 150 °C for 24 h, and cooled to room temperature (RT) at 6 °C hr^{-1}. The product contained aggregated violet block-shaped crystals. However, the powder X-ray diffraction (PXRD) pattern of the product confirmed a mixture was formed (see Figure 2). The major phase, subsequently determined to be $VO(SeO_2OH)_2$ by single crystal X-ray diffraction (see below), was found in nearly 90% yield based on V_2O_5. We were unable to identify the minor phases in the PXRD; however, these phases are soluble in hot water. Thus, the as synthesized product was ground and placed in hot water to dissolve any soluble impurities. The recovered product was washed with excess amounts of distilled water and acetone, and was confirmed as $VO_2(SeO_2OH)_2$ by powder X-ray diffraction (PXRD). The calculated and experimental X-ray diffraction patterns are in excellent agreement as shown in Figure 2. We found that the molar ratio (m) of SeO_2/V_2O_5 is critically important to synthesize pure phase $VO_2(SeO_2OH)_2$. With $m < 4$, $VOSeO_3 \cdot H_2O$[24] was produced as a major phase and, in addition, an excess amout of oxalic acid leads to the formation of elemental Se, as confirmed by PXRD analyses.

(20) Kim, S.-H.; Halasyamani, P. S.; Melot, B. C.; Seshadri, R.; Green, M. A.; Sefat, A. S.; Mandrus, D. *Chem. Mater.* **2010**, *22*, 5074.
(21) Ginsberg, A. P. *Inorg. Chim. Acta, Rev.* **1971**, *5*, 45.
(22) Hay, P. J.; Thibeault, J. C.; Hoffmann, R. *J. Am. Chem. Soc.* **1975**, *97*, 4884.
(23) Greenwood, N. N.; Earnshaw, A. *Chemistry of the Elements*, 2nd ed.; Butterworth-Heinemann: Oxford, 1997.

(24) Huan, G.; Johnson, J. W.; Jacobson, A. J.; Goshorn, D. P.; Merola, J. S. *Chem. Mater.* **1991**, *3*, 539.
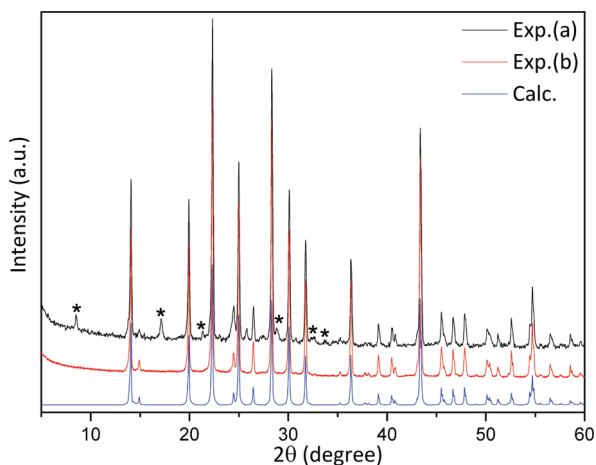
Figure 2. Experimental and calculated PXRD patterns. The PXRD patterns of the product taken before and after the washing step are drawn as black- and red-solid lines, respectively. The asterisk (*) indicates unidentified reflections from impurity phases. The blue-solid line is the calculated PXRD pattern from our refined single crystal data.

Table 1. Crystallographic Data for VOHO(SeO$_2$)$_2$

formula	VO(SeO$_2$OH)$_2$
fw (g/mol)	322.88
T (K)	296.0(2)
λ (Å)	0.71073
crystal system	tetragonal
space group	$P\bar{4}2_1c$ (No. 114)
a (Å)	8.9181(3)
c (Å)	7.9708(6)
V (Å^3)	633.94(6)
Z	4
ρ_{calcd} (g/cm^3)	3.38
μ (mm^{-1})	13.029
$2\theta_{max}$ (deg)	57.6
R (int)	0.0273
GOF (F^2)	0.905
$R(F)^a$	0.0186
$R_w(F_o^2)^b$	0.0303
Flack param.	−0.010(11)

$^a R(F) = \sum||F_o| - |F_c||/\sum|F_o|.$ $^b R_w(F_o^2) = [\sum w(F_o^2 - F_c^2)^2/\sum w(F_o^2)^2]^{1/2}.$

Single Crystal X-ray Diffraction. A violet block-shaped crystal (0.03 × 0.03 × 0.09 mm^3) was chosen for single-crystal data collection. The data were collected using a Siemens SMART APEX diffractometer equipped with a 1K CCD area detector using graphite-monochromated Mo Kα radiation. A hemisphere of data was collected using a narrow-frame method with scan widths of 0.30° in ω, and an exposure time of 60s per frame. The data were integrated using the Siemens SAINT program[25] with the intensities corrected for Lorentz-Polarization, air absorption, and absorption attributable to the variation in the path length through the detector face plate. ψ-scans were utilized for the absorption correction on the data.[25] The data were solved by direct methods and refined against F^2 by full-matrix least-squares techniques using SHELXS-97 and SHELXL-97, respectively.[26] All of the atoms in the structure were refined with anisotropic thermal parameters, and the refinements converged

(25) *SAINT*, 4.05 ed.; Siemens Analytical X-ray Systems, Inc.: Madison, WI, 1995.
(26) Sheldrick, G. M. *SHELXL-97 - A program for crystal structure refinement*; University of Göttingen: Göttingen, Germany, 1997.
(27) Spek, A. L. *PLATON*; Utrecht University: Utrecht, The Netherlands, 2001.

Table 2. Atomic Coordinates and Equivalent Isotropic Displacement Parameters (Å^2 × 10^3) for VO(SeO$_2$OH)$_2$

	x	y	z	U_{eq}^a	occ.
V(1)	0	0.5	0.19612(8)	9(1)	0.924(1)
V(2)	0	0.5	0.3042(9)	14(2)	0.076(1)
Se(1)	0.79107(3)	0.20768(3)	0.22444(3)	13(1)	1.0
O(1)	0	0.5	−0.0044(2)	20(1)	1.0
O(2)	0.8112(3)	0.3932(2)	0.2495(2)	18(1)	1.0
O(3)	0.6071(2)	0.1928(2)	0.2631(2)	16(1)	1.0
O(4)	0.8544(2)	0.1463(2)	0.4244(3)	25(1)	1.0
H(1)	0.921(3)	0.169(4)	0.437(4)	44(11)	1.0

$^a U_{eq}$ is defined as a third of the trace of the orthogonalized $\mathbf{U}_{ij}$ tensor.

Table 3. Selected Bond Distances (Å) in VO(SeO$_2$OH)$_2$

V(1)−O(1)	1.5980(15)	V(2)−O(1)	1.526(8)
V(1)−O(2) × 2	1.981(2)	V(2)−O(2) × 2	1.983(3)
V(1)−O(3) × 2	1.993(2)	V(2)−O(3) × 2	2.038(3)
V(1)−O(1)	2.3874(15)	V(2)−O(1)	2.459(8)
Se−O(2)	1.676(2)	H(1)−O(4)	0.64(3)
Se−O(3)	1.675(2)		
Se−O(4)	1.7772(17)		

for $I > 2\sigma(I)$. The Flack parameter refined to −0.01(1). The structure was checked for missing symmetry elements using PLATON.[27] Relevant crystallographic data, atomic coordinates and thermal parameters, and selected bond distances and angles for VO(SeO$_2$OH)$_2$ are given in Tables 1, 2, and 3, respectively.

Powder X-ray Diffraction. The PXRD data were collected on a PANalytical X'pert pro diffractometer using Cu Kα radiation in the 2θ range 5−90°. A step size of 0.008 degrees (deg) with a scan time of 0.3 s/deg were used.

Magnetic Measurements. For the magnetic measurements, a Quantum Design Magnetic Property Measurement System (MPMS) was utilized. Direct current (DC) magnetization measurements were performed with ∼23 mg of the powder sample, loaded in a diamagnetic capsule. The field cooled magnetizations for a warming cycle were measured at 50 and 1000 Oe from 1.8 K to 350 K. The magnetic hysteresis curve was measured at 2 K by sweeping the applied magnetic field from −7 to 7 T(T).

Thermogravimetric Analysis. Thermogravimetric analysis (TGA) was performed on a TGA 951 thermogravimetric analyzer (TA Instruments). The sample (∼ 20.0 mg) was placed in a platinum crucible and heated at a rate of 10 °C min^{-1} from room temperature to 800 °C in flowing N$_2$.

UV−vis Diffuse Reflectance Spectroscopy. UV−visible reflectance data were collected on a Varian Cary 500 scan UV−vis−NIR spectrophotometer over the 200−1500 nm spectral range at room temperature. Poly(tetrafluoroethylene) was used as a reference material. The reflectance spectrum was converted to absorbance using the Kubelka−Munk function.[28,29]

Second Harmonic Generation (SHG). We performed powder SHG measurements on a modified Kurtz-NLO[30] system using a pulsed Nd:YAG laser with a wavelength of 1064 nm. A detailed description of the equipment and methodology has been published.[31] The sample was ground and sieved into distinct particle size ranges (20−45, 45−63, 63−75, 75−90, > 90 μm) because of size-dependent SHG efficiency.[30] To make relevant

(28) Kubelka, P.; Munk, F. Z. *Tech. Phys.* **1931**, *12*, 593.
(29) Tauc, J. *Mater. Res. Bull.* **1970**, *5*, 721.
(30) Kurtz, S. K.; Perry, T. T. *J. Appl. Phys.* **1968**, *39*, 3798.
(31) Ok, K. M.; Chi, E. O.; Halasyamani, P. S. *Chem. Soc. Rev.* **2006**, *35*, 710.

comparisons with known SHG materials, crystalline α-SiO₂ and LiNbO₃ were also ground and sieved into the same particle size ranges. No index matching fluid was used in any of the experiments.

Computational Details. A disorder free structure was adopted for the calculations, that is, full occupancy on V(1) was assumed (see Table 2). First principles density functional theory (DFT)[32,33] electronic band structure calculations for VO(SeO₂OH)₂ were performed with the plane wave pseudopotential method.[34] As implemented in the Quantum ESPRESSO (4.0.1 version) package,[35] ultrasoft pseudopotentials (USPPs)[36] were utilized with the Perdew−Burke−Ernzerhof (PBE) exchange-correlation functional of a generalized gradient approximation (GGA)[37] for the exchange-correlation corrections. On-site repulsion was employed in GGA+U method[38] to properly take into consideration the electron correlation in the V 3d states. Here, the effective U_{eff} parameter of 2 and 3 eV on the V atom was adopted. A plane wave energy cutoff was set to 37 Ry. The k-point grid of $4 \times 4 \times 6$ was used for the Brillouin zone integrations with a Gaussian smearing of 0.01 Ry. A total energy convergence threshold set to 10^{-6} Ry indicated self-consistency.

Results and Discussion

Structure. VO(SeO₂OH)₂ crystallizes in the noncentrosymmetric space group $P\bar{4}2_1c$ (No. 114) that is in crystal class $\bar{4}2m$, a non-chiral and non-polar crystal class (see Table 1).[39] VO(SeO₂OH)₂ exhibits a three-dimensional structure, consisting of chains of corner-shared VO₆ octahedra that run parallel to the c-axis. The chains are connected by the SeO₂OH group (see Figure 1). The V⁴⁺ cation is statistically disordered over two sites, V(1) and V(2), with 92.4(1)% and 7.6(1)% occupancies, respectively (see Table 2). In connectivity terms, the structure can be written as $\{[VO_{6/2}]^{2-} 2[SeO_{2/2}(OH)_{1/1}]^{1+}\}^0$. The V−O and Se−O bond distances range from 1.594(2) to 2.391(2) Å and 1.674(2) to 1.777(2) Å, respectively, and bond valence calculations[40,41] resulted in values 4.16 and 3.98 for V⁴⁺ and Se⁴⁺, respectively.

The thermal stability of VO(SeO₂OH)₂ was investigated through thermogravimetric measurements (see Supporting Information, Figure S1). VO(SeO₂OH)₂ begins to decompose at ∼130 °C by releasing 1 mol of H₂O (Exp: 94.7%; Calcd: 94.7%). Two additional steps were observed at ∼330 °C and ∼410 °C attributable to SeO₂ loss (Exp.: 68.0%; Calcd 68.7%). Finally, VO₂ remains as confirmed by PXRD.

The UV−vis diffuse reflectance data as shown in Supporting Information, Figure S2 reveals that the optical
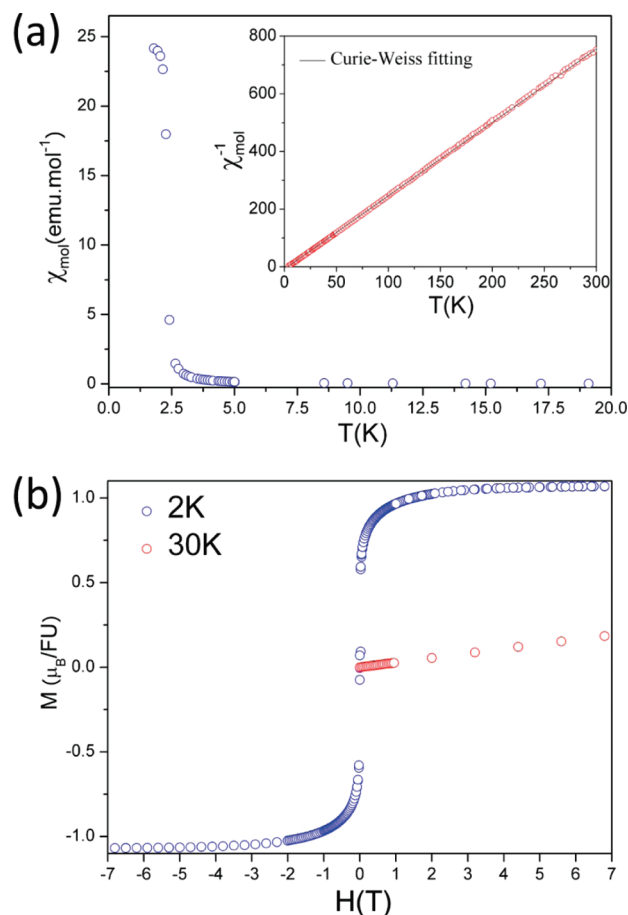

Figure 3. (a) Molar magnetic susceptibility (χ_{mol}) of VO(SeO₂OH)₂ curves measured at 50 Oe (blue-open circles). Inset shows χ_{mol}^{-1} measured at 1000 Oe (red-open circle) with a Curie−Weiss fit (black solid line) from 5−300 K. (b) The magnetic hysteresis curves measured at 30 K (red-open circles) and 2 K (blue-open circles) in external magnetic fields from 0−7 T and from −7 to +7 T, respectively.

band gap energy of approximately 2.9 eV and the three peaks seen in the region of 1.2−2.3 eV attributable to d−d transitions of the V⁴⁺ cations.

Powder second-harmonic generating measurements[30,31] revealed an efficiency comparable to α-SiO₂. The weak SHG is not unexpected as VO(SeO₂OH)₂ is neither polar nor chiral. Although some of the local polarity is present, for example, the SeO₃ polyhedra and distorted VO₆ octahedra, the individual polarizations are directed in opposite directions resulting in a macroscopically non-polar material. In addition, there is no chirality, that is, "handedness", associated with VO(SeO₂OH)₂. The cancellation of the local polarity, in conjunction with the lack of chirality, results in a weak SHG efficiency.

DC Magnetization Measurements. The temperature dependent dc-magnetization measurements were performed in the range of 2−350 K under magnetic fields of 50 and 1000 Oe. Figure 3a shows the temperature dependent molar susceptibility (χ_{mol} vs T) curve measured at 50 Oe where a ferromagnetic transition is clearly exhibited below ∼4 K. Above 4 K, the χ_{mol}^{-1} at 1000 Oe (see inset in Figure 3a) fits well to a modified Curie−Weiss equation given as $C/(T - \Theta_{CW}) + \chi_0$ where C, Θ_{CW}, and χ_0 represent the Curie constant, the Weiss temperature, and

(32) Hohenberg, P.; Kohn, W. *Phys. Rev.* **1964**, *136*, B864.
(33) Kohn, W.; Sham, L. J. *Phys. Rev.* **1965**, *140*, A1133.
(34) Pickett, W. E. *Comput. Phys. Rep.* **1989**, *9*, 115.
(35) Baroni, S.; Corso, A. D.; Gironcoli, S. d.; Giannozzi, P.; Cavazzoni, C.; Ballabio, G.; Scandolo, S.; Chiarotti, G.; Focher, P.; Pasquarello, A.; Laasonen, K.; Trave, A.; Car, R.; Marzari, N.; Kokalj, A. *Quantum ESPRESSO package*, 4.0.1 version; http://www.quantum-espresso.org/.
(36) Vanderbilt, D. *Phys. Rev. B* **1990**, *41*, 7892.
(37) Perdew, J. P.; Burke, K.; Ernzerhof, M. *Phys. Rev. Lett.* **1996**, *77*, 3865.
(38) Anisimov, V. I.; Zaanen, J.; Andersen, O. K. *Phys. Rev. B* **1991**, *44*, 943.
(39) *International Tables for Crystallography*; Hahn, T., Ed.; Kluwer Academic: Dordrecht, Holland, 2006; Vol. A, Space Group Symmetry.
(40) Brown, I. D.; Altermatt, D. *Acta Crystallogr.* **1985**, *B41*, 244.
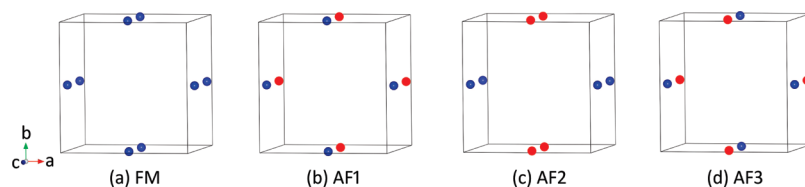(41) Brese, N. E.; Okeeffe, M. *Acta Crystallogr.* **1991**, *B47*, 192.

Figure 4. Schematic representations of the four different spin states. For clarity, only the V sites are shown with blue-filled circles (up-spin) and red-filled circles (down-spin).

Table 4. Relative Energies (eV/FU) of Four Different Magnetic States of VO(SeO$_2$OH)$_2$

states	ΔE (meV/FU)		M_{Tot} (μ_B/FU)
	$U_{eff} = 2$ eV	$U_{eff} = 3$ eV	
FM[a]	0	0	1
AF1	0.33	0.41	0
AF2	0.29	0.13	0
AF3	0.62	0.54	0

[a] Indicates the calculated ground state whose total energy set to 0 eV.

a temperature independent term, respectively. From the Curie–Weiss fit, an effective magnetic moment (μ_{eff}) value of ~1.74(1) μ_B per V^{4+} was estimated that is in good agreement with the theoretical spin-only value of 1.73 μ_B per V^{4+}. The Weiss temperature and the temperature independent term estimated are of 3.87(1) K and $1.8(3)\times10^{-4}$ emu mol^{-1} Oe^{1-}, respectively. As mentioned, the molar susceptibility, χ_{mol}, deviates from Curie–Weiss behavior below ~4 K, as seen in the $1/\chi_{mol}$ vs T curve. The deviation is attributable to the ferromagnetic spin alignment of the unpaired electron on the V^{4+} at $T_C = \sim$ 2.5 K. Isothermal magnetization curves were measured at 2 and 30 K (see Figure 3b). The magnetization curve measured at 30 K changes linearly in the paramagnetic state. The magnetic hysteresis curve measured at 2 K reveals soft ferromagnetic behavior with a saturated magnetic moment of 1.09 μ_B/FU that is also consistent with the full spin alignment of the unpaired electron on the V^{4+}.

Electronic Band Structures. The first principles DFT electronic band structures were carried out for VO(SeO$_2$OH)$_2$ with four different magnetic states using the GGA+U method where U_{eff} was set at 2 and 3 eV. It should be noted that the GGA+U method would not be appropriate if the filled V 3d orbitals in VO(SeO$_2$OH)$_2$ exhibited any orbital degeneracy. Such orbital degeneracy is not allowed attributable to the distorted VO$_6$ octahedra in the structure. Also, it is noted that the spin polarized state calculations with GGA alone result in metallic states for VO(SeO$_2$OH)$_2$.[20] In order to investigate the theoretical ground state, we considered a ferromagnetic and three antiferromagnetic (AF1, AF2, AF3) states, as shown in Figure 4, where their magnetic unit cells are equivalent to the crystal structure. The relative total energies of the four spin states (Figure 4) with two different U_{eff} values are listed in the Table 4 where the ferromagnetic (FM) state energy was set to zero. The calculations indicate that the calculated ground state is a ferromagnetic state, consistent with our magnetic experiments.
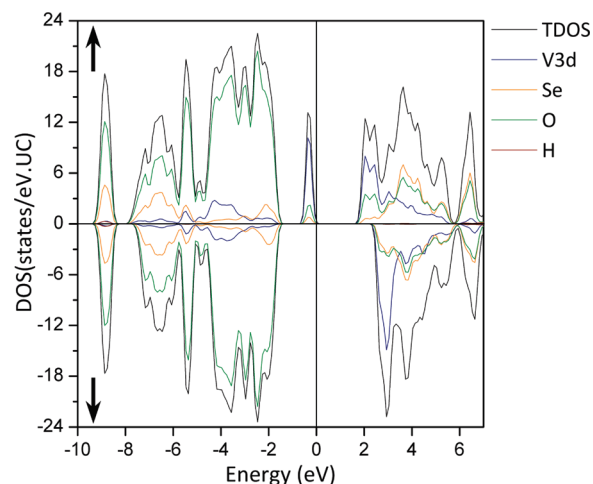

Figure 5. TDOS (black solid line) and PDOSs of V 3d (blue solid line), Se (yellow solid line), O (green solid line), and H (brown solid line) of VO(SeO$_2$OH)$_2$ in the ferromagnetic (FM) state calculated using the Quantum-Espresso code. Up(down)-spin channel is seen in the upper (lower) panel with the Fermi level set at 0 eV.

The total and projected density of states, TDOS and PDOS, respectively, of the FM state were calculated with $U_{eff} = 2$ eV using the Quantum-Espresso code (ver. 4.0.1) (see Figure 5).[35] As shown in Figure 5, an energy band gap exhibited at the Fermi level is also in agreement with the insulating nature of the title material. Below near −1.5 eV, the up- and down-spin DOSs are almost identical to each other, indicative of the weak spin polarization. However, only one up-spin DOS peak appears near −0.7 eV to E_F where the PDOSs reveals predominant contributions of V 3d orbitals and weak contributions of O 2sp and Se sp orbitals. Further detailed PDOSs examinations confirmed that the V 3d is solely V 3d$_{xy}$ where the Cartesian axes, x and y, are parallel to the equatorial V−O bonds. Also, only the axial O(1) contribution is negligible in the up-spin DOS peak. From these results, it is reasonable to probe the magnetic moments primarily localized on the V^{4+} cation whose spin polarizations induce the spin polarizations on the non-magnetic ions with distinguishable *intra-* and *inter*-chain spin polarization paths that are mainly distinct below −1.5 eV and above to E_F, respectively, in the electronic structure.

To examine the spin polarizations of VO(SeO$_2$OH)$_2$, we initially performed spin polarization density calculations using the pseudopotential method. Figures 6a and 6b reveal the total and partial spin polarization density isosurfaces, respectively. The spin polarization density, $\rho_S(r)$, is defined as $\rho_S(r) = \rho_\uparrow(r) - \rho_\downarrow(r)$ where $\rho_\uparrow(r)$ and $\rho_\downarrow(r)$ indicate spin-up and spin-down densities, respectively.
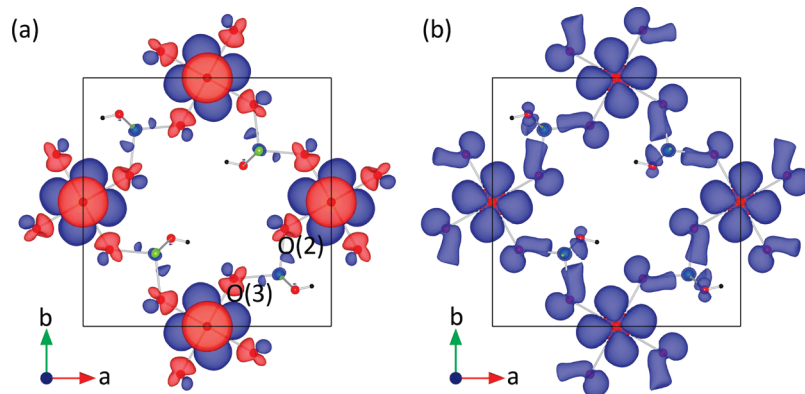
Figure 6. Total and partial spin polarization density (-1.5 eV to E_F) isosurfaces in (a) and (b), respectively, plotted at 1.4×10^{-3} e$^-$/Å^3 for VO(SeO$_2$OH)$_2$ calculated using the Quantum-Espresso code. For clarity, one layer of VO(SeO$_2$OH)$_2$ is chosen from $0c$ to $+0.5c$. The blue (red) color indicates positive (negative) spin polarization.
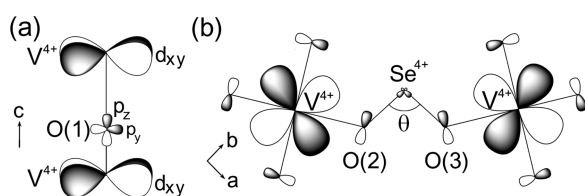

Figure 7. (a) *Intrachain* O(1)−V−O(1) orbital interaction (the O(1) p_x orbital is not shown for clarity) along the c-direction. Note that the total orbital overlap is zero. (b) *Interchain* SSE magnetic orbital interactions in the ab-plane via V−O(2)−Se−O(3)−V.

The total spin polarization isosurface plotted shows larger positive isosurfaces on the V^{4+} cations that resemble the density of the $3d_{xy}$ orbital[42,43] because only the up-spin $3d_{xy}$ orbital is fully occupied. The complex patterns of the induced spin polarizations are observed in the other atoms. In particular, relatively larger negative spin polarizations are induced on the axial O(1) atom (see Table 4). This induced polarization on O(1) is associated with magnetic interactions in the [−V−O(1)−V−] linear chain where there are negligible orbital overlap integrals between the magnetic orbital and the O(1) 2sp orbitals (see Figure 7a). Thus, antiferromagnetic superexchange (SE) interactions[16−18] are suppressed that result in favorable *ferromagnetic* interactions between the intrachain V^{4+} cations. Likewise, the nearly equivalent spin polarization on the V^{4+} is shown in the partial spin polarization density isosurface calculated from -1.5 eV to E_F (see Figure 6b). As mentioned above, attributable to the negligible contribution of the axial O(1) atom, the isosurfaces reveal interchain magnetic interactions (although the magnetic interactions are complex) as the magnetic cations are connected by the non-magnetic SeO$_2$OH group. In fact, the isosurface is equivalent to the total electron density isosurface in the energy region where the down-spin DOS is negligible (see Figure 5). Interestingly, the plot shows the positively spin polarized lobes along on the O(2)−Se^{4+}−O(3) that correspond to σ-type bonding characteristics of the lone-pair group. Therefore, a plausible magnetic interaction pathway is the shortest pathway,
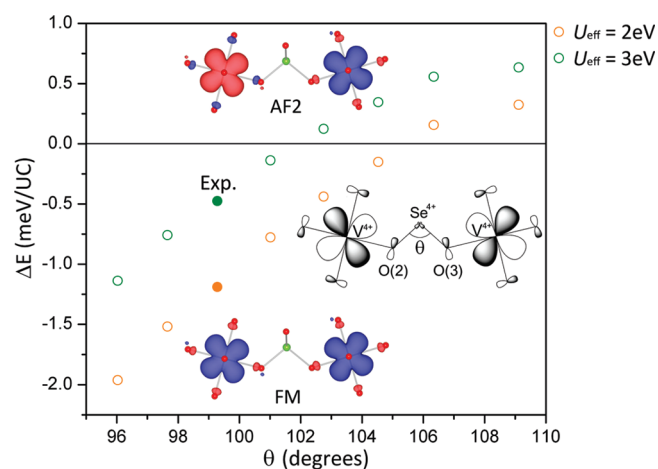

Figure 8. Relative energy (ΔE) regarding the *inter*-chain magnetic interactions with respect to the O(2)−Se−O(3) angle (θ) calculated at $U_{eff} = 2$ (orange circles) and 3 eV (green circles). The two filled circles indicate the experimentally determined O(2)−Se−O(3) angle of 99.3(1)°. The upper and lower spin polarization density isosurface plots at 4.5×10^{-2} e$^-$/Å^3 indicate FM and AF2 states with $U_{eff} = 2$ eV, respectively, calculated using the Quantum-Espresso code.

V^{4+}−O(2)−Se^{4+}−O(3)−V^{4+}(see Figure 7b), where all of the ions are almost in the same plane. The magnetic orbital of V^{4+} in the VO$_6$ octahedron is well described.[44] An interesting question is how the magnetic orbitals result in magnetic interactions mediated through Se^{4+} cations, that is, interchain magnetic interactions. In this regard we initially speculated that the interchain magnetic interaction, specifically, supersuper exchange (SSE) interactions, might be susceptible to structural variations[45,46] in terms of the O(2)−Se−O(3) angle since M−O−M angle dependent SE interactions are well understood on edge-shared MO$_6$ octahedra.[47]

To describe how critically the SSE interactions are dependent on the O(2)−Se−O(3) angle, we performed angle-dependent DFT calculations with $U_{eff} = 2$ and 3 eV

(42) Seo, D.-K. *J. Chem. Phys.* **2006**, *125*, 154105/1.
(43) Seo, D.-K. *J. Chem. Phys.* **2007**, *127*, 184103/1.

(44) Wheeler, R. A.; Whangbo, M. H.; Hughbanks, T.; Hoffmann, R.; Burdett, J. K.; Albright, T. A. *J. Am. Chem. Soc.* **1986**, *108*, 2222.
(45) Koo, H.-J.; Whangbo, M.-H.; VerNooy, P. D.; Torardi, C. C.; Marshall, W. J. *Inorg. Chem.* **2002**, *41*, 4664.
(46) Whangbo, M.-H.; Koo, H.-J.; Dai, D. *J. Solid State Chem.* **2003**, *176*, 417.
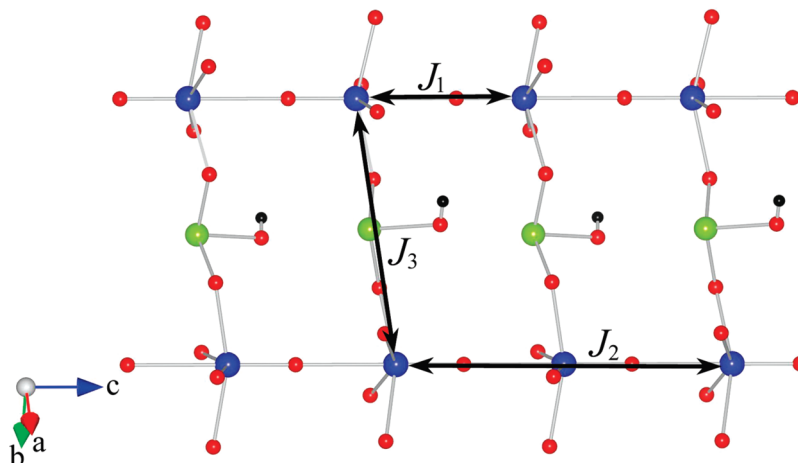(47) Kahn, O. *Molecular Magnetism*; Wiley-VCH Inc.: New York, 1993.

Figure 9. Two *intra*-chain magnetic interactions given as J_1, and J_2 and one *inter*-chain magnetic interaction given as J_3 are drawn.

for FM and AF2 states whereby the O(2)−Se−O(3) angle ranges from 96−109°. Note that the experimentally determined O(2)−Se−O(3) angle is 99.3(1)° and each *intra*-chain magnetic interaction is ferromagnetic in both spin states. Figure 8 shows the relative energy (ΔE) plots with respect to the O(2)−Se−O(3) angle (θ) where ΔE is defined as $E_{FM} - E_{AF2}$ in meV per unit cell (/UC) with respect to *interchain* magnetic interactions. It should be noted that at each point in Figure 8, the bond valence sum for Se^{4+} was close to 4.0, indicating that in changing the O(2)−Se−O(3) angle, the Se−O bond distances were chemically reasonable. The plots reveal a remarkable feature in that the SSE interactions are O(2)−Se−O(3) angle dependent, that is, the FM state becomes less stable as the angle increases and eventually the AF2 state becomes stable. In other words, the *antiferromagnetic* interchain interactions are enhanced as the O(2)−Se−O(3) angle increases. From the calculations, the *ferromagnetic* interchain interactions are favored between 96−105° and 96−102° at U_{eff} = 2 and 3 eV, respectively. This feature resulting from the *competition*, ferromagnetic versus antiferromagnetic interactions, is quite analogous to what is observed in edge-shared M_2O_8 octahedra or edge-shared M_2O_6 squares such as $[Cu_2O_6]^{42-47}$ where the increased M−O−M angle from 90° provides nonzero magnetic orbital overlap integrals that enhance the favorable antiferromagnetic interactions, that is, the GK rules. The relevance of the orbital overlap integrals on Se sp orbitals (see Figure 7b) is observed, analogous to GK rules. Consequently, antiferromagnetic SSE interactions are favored with the increased O(2)−Se−O(3) angle. This interpretation supports the experimental magnetic measurements as V(1) and V(2) are almost on the same plane of O(2)−Se^{4+}−O(3). It is also of interest to compare the magnetic behavior of VO(SeO$_2$OH)$_2$ with Pb$_2$A$_2$VO$_9$ (A = V^{5+} or As^{5+})[48]

(48) Mentre, O.; Koo, H. J.; Whangbo, M. H. *Chem. Mater.* **2008**, *20*, 6929.
(49) Bombardi, A.; Rodriguez-Carvajal, J.; Matteo, S. D.; Bergevin, F. d.; Paolasini, L.; Carretta, P.; Millet, P.; Caciuffo, R. *Phys. Rev. Lett.* **2004**, *93*, 027202/1.
(50) Rosner, H.; Singh, R. R. P.; Zheng, W. H.; Oitmaa, J.; Drechsler, S. L.; Pickett, W. E. *Phys. Rev. Lett.* **2002**, *88*, 186405/1.

Table 5. Magnetic Moments on V^{4+}, Se^{4+}, and O^{2-} in the Ferromagnetic State of VO(SeO$_2$OH)$_2$ with U_{eff} = 2 and 3 eV Calculated Using Quantum-Espresso

U_{eff} (eV)	V	Se	O(1)	O(2)	O(3)	O(4)	H
2	1.1463	0.0197	−0.1627	−0.0077	−0.0102	0.0016	0.0002
3	1.1898	0.0216	−0.1807	−0.016	−0.017	0.0016	0.0002

and Li$_2$VOTO$_4$ (T = Si^{4+} or Ge^{4+}),[49,50] where a stereo-active lone-pair is *not* observed. In both of Pb$_2$A$_2$VO$_9$ and Li$_2$VOTO$_4$, the SSE magnetic interactions between the V^{4+} cations are mediated through either A^{5+} or T^{4+}, cations that do *not* have a stereoactive lone-pair. Each AO$_4$ and TO$_4$ tetrahedron has a O$_{eq}$−T−O$_{eq}$ angle of 109.0(2)° and O$_{eq}$−A−O$_{eq}$ angle of 106.3(4)−107.1(6)° where O$_{eq}$ is bonded to V^{4+}. Thus the antiferromagnetic SSE interactions are enhanced resulting in favorable antiferromagnetic interactions, as is experimentally observed.[48−50] Consequently, the lone-pair on Se^{4+} in VO(SeO$_2$OH)$_2$ *decreases* the O(2)−Se−O(3) angle to 99.3(1)°, *reducing* the antiferromagnetic SSE interactions, and is the driving force *favoring* the ferromagnetic behavior. Thus, the ferromagnetic behavior in VO(SeO$_2$OH)$_2$ is attributable to the reduced antiferromagnetic SE and SSE interactions caused by the negligible orbital overlap integral and the smaller O(2)−Se−O(3) angle, respectively.

Finally, the magnetic exchange parameters were estimated using the total energies of the four spin states as listed in Table 4. As the magnetic exchanges are mediated through chemical bonds, we consider the magnetic exchange interactions, J_1, and J_2 as the nearest and next nearest magnetic exchange interactions in the chain and J_3 as the magnetic *inter*-chain interaction (see Figure 9). The relevance of J_2 may be supported by the largest induced magnetic moments of O(1) (see Table 5).[44] The energies of the four ordered magnetic states can be written in terms of spin Hamiltonian,

$$H = -\sum_{i<j} J_{ij}\hat{S}_i \cdot \hat{S}_j$$

where J_{ij} ($= J_1$, J_2, and J_3) is the magnetic exchange parameter for the pairwise magnetic interaction between the magnetic sites i and j, and $\hat{S}_i$ and $\hat{S}_j$ are the spin

Table 6. Estimated Magnetic Exchange Parameters (meV) from the GGA+U (U_{eff} = 2 and 3 eV) Calculations

U_{eff} (eV)	J_1	J_2	J_3
2	0.33	−0.62	0.15
3	0.41	−0.54	0.07

angular momentum operators at the magnetic sites i and j, respectively. When $J > 0$, a ferromagnetic interaction is favored. The total magnetic exchange energy of the four spin states can be described as

$$E_{FM} = \frac{N^2}{4}(-2J_1 - 2J_2 - 4J_3)$$

$$E_{AF1} = \frac{N^2}{4}(2J_1 - 2J_2 - 4J_3)$$

$$E_{AF2} = \frac{N^2}{4}(-2J_1 - 2J_2 + 4J_3)$$

$$E_{AF3} = \frac{N^2}{4}(2J_1 - 2J_2 + 4J_3)$$

where N defined as unpaired electrons per magnetic site is 1.[51,52] Using the equations above, the magnetic exchange parameters of J_1, J_2, and J_3 may be expressed as

$$
\begin{aligned}
J_1 &= -E_F + E_{AF1} \\
&= -E_{AF2} + E_{AF3} \\
J_2 &= -E_F - E_{AF3} \\
&= -E_{AF1} - E_{AF2} \\
J_3 &= \frac{1}{2}(-E_F + E_{AF2}) \\
&= \frac{1}{2}(-E_{AF1} + E_{AF3})
\end{aligned}
$$

and are summarized in Table 6. The magnitudes of J_1 and J_2 are larger than that of J_3. As expected, J_3 is ferromagnetic. Interestingly, J_1 and J_2 have opposite signs that may result in a weak ferromagnetic *intra*-chain interaction.[48] Overall, the

(51) Dai, D.; Whangbo, M.-H. *J. Chem. Phys.* **2003**, *118*, 29.
(52) Dai, D.; Whangbo, M.-H. *J. Chem. Phys.* **2001**, *114*, 2887.

small values of J_1 and J_2 are anticipated from the orientation of the V 3d$_{xy}$ orbitals that are not pointing toward each other along the chain, and a small J_3 is attributed by the magnetic interactions between the chains that are mediated through the complex non-magnetic SeO$_2$OH group. In addition, the small J-values are also consistent with the very low Curie temperature ($T_C \sim 2.5$ K) and the small Weiss temperature (Θ_{CW} = 3.87(1) K). As mentioned above, J_3 is the magnetic *inter*-chain interaction that is dependent on the O(2)−Se−O(3) angle because J_3 is also defined as one-half of the relative energy (ΔE) with the opposite sign.

Conclusion

In summary, we have successfully synthesized and characterized a novel *acentric ferromagnetic* material VO(SeO$_2$OH)$_2$ with $T_C = \sim 2.5$ K, by using oxalic acid dihydrate as a reducing agent. Such acentric ferromagnetic materials are rare. The novel structural features result in reduced antiferromagnetic SE and SSE interactions in the *intra*- and *inter*-chain pathways, respectively, attributable to the negligible orbital overlap integrals between the V 3d$_{xy}$ and the O(1) 2sp orbitals, and the small orbital overlap integrals on Se sp orbitals. Specifically, the O(2)−Se−O(3) angular dependence on the magnetic *inter*-chain interaction is described through an extension of the GK rules. In addition, it is demonstrated, for the first time, that the stereoactive lone-pair on Se^{4+} is the driving force favoring the *inter*-chain ferromagnetic interactions.

Supporting Information Available: Further details are given in Figures S1−S3. Crystallographic data is given in CIF format. This material is available free of charge via the Internet at http://pubs.acs.org.